Supporting information for

Stable high-Q bouncing ball modes inside a Fabry-Pérot cavity

Xiaoqin Wu[1†], Qiushu Chen[1†], Yipei Wang[2], Xiaotian Tan[1] and Xudong Fan[1*]

[1]Department of Biomedical Engineering, University of Michigan, 1101 Beal Avenue, Ann Arbor, Michigan 48109, USA

[2]Department of Electrical Engineering and Computer Science, University of Michigan, Ann Arbor, MI 48109, USA

†Equal contribution

*xsfan@umich.edu

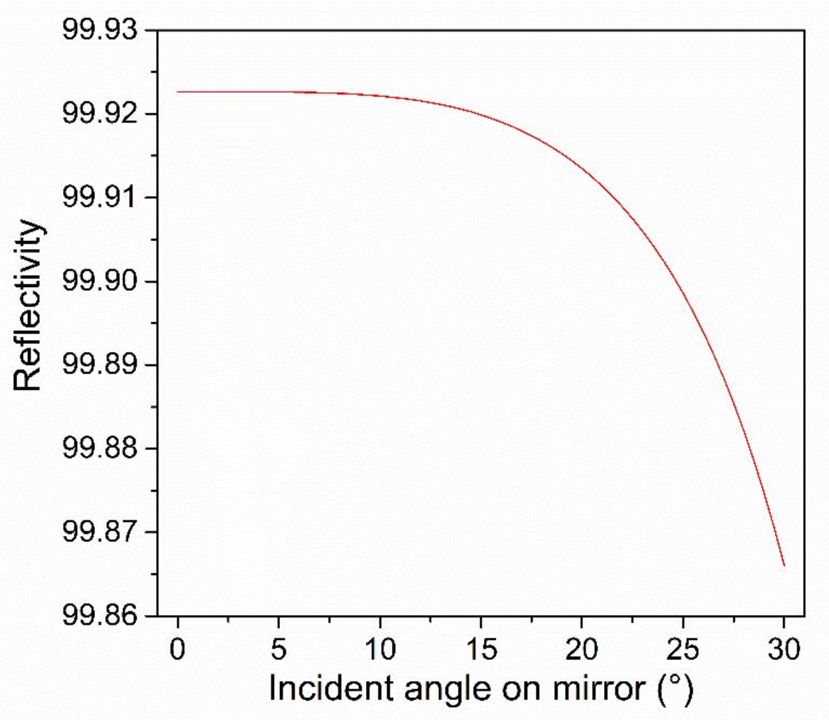

Figure S1. Calculated reflectivity of a 15-layer dielectric mirror as a function of the incident angle using an example model named “Distributed Bragg Reflector” in COMSOL.

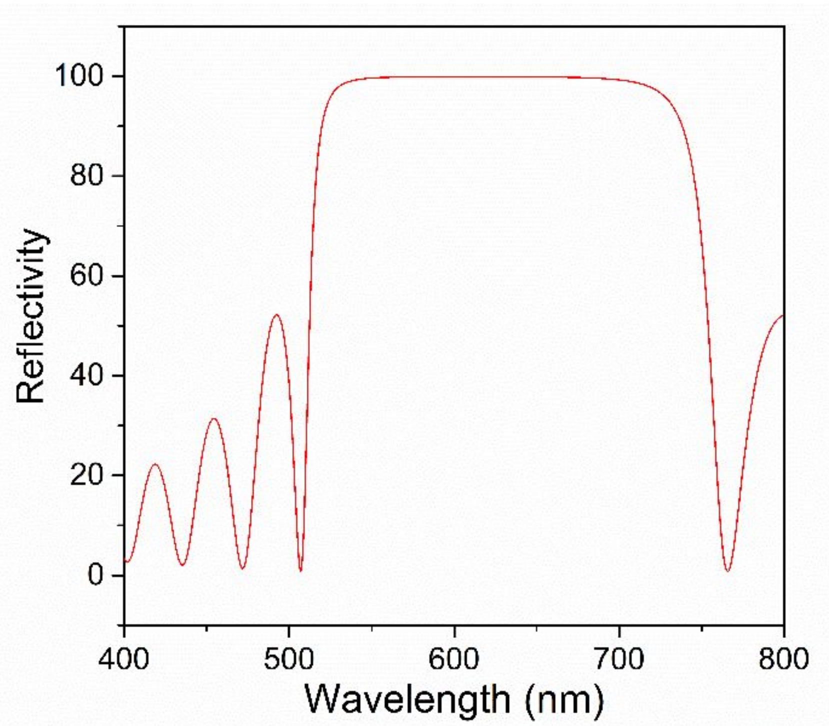

Figure S2. Calculated reflectivity of a 15-layer dielectric mirror as a function of the optical wavelength using an example model named “Distributed Bragg Reflector” in COMSOL. The center optical wavelength is set as 610 nm.

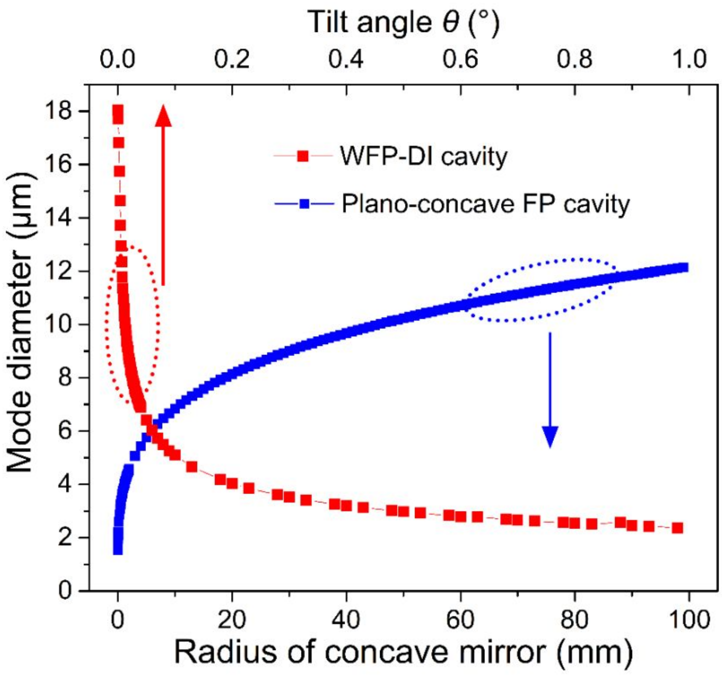

Figure S3. Calculated mode diameter w_1 of a plano-concave FP cavity as a function of the radius of the concave mirror R (blue squares) and the effective mode size w_2 of the 1st order transverse mode for a WFP-DI cavity as a function of the tilt angle (red squares).

w_1 is calculated by

$$w_1 = \left(\frac{d\lambda}{\pi}\right)^{1/2}\left(\frac{1}{g(1-g)}\right)^{1/4}, \text{ and } g = 1-\frac{d}{R}.$$

w_2 is calculated in COMSOL by

$$w_2 = \frac{\left(\int \varepsilon |E|^2 \, dx\right)^2}{\int (\varepsilon |E|^2)^2 \, dx},$$

where the integration is chosen to be the line across the vertical center of the freestanding wave node closest to the bottom mirror (e.g., y = 0.122 μm).

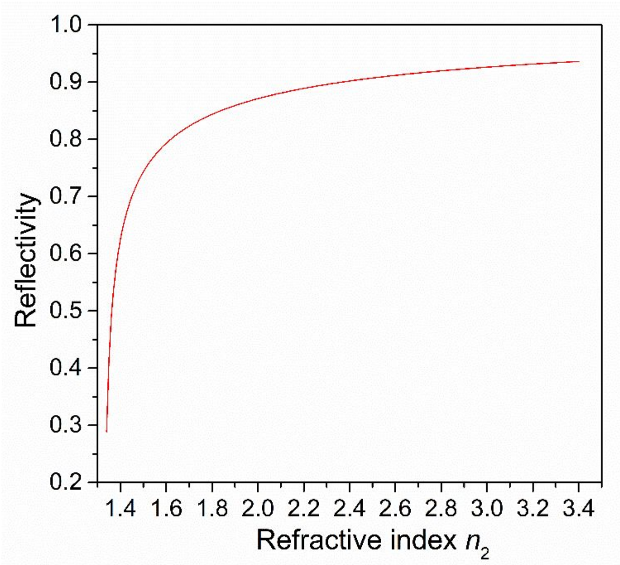

Figure S4. Calculated reflectivity of the dielectric interface as a function of the surrounding medium RI n_2, at fixed n_1 = 1.33, using the Fresnel equations and an incident angle γ = 87.8º with s-polarization as an example.

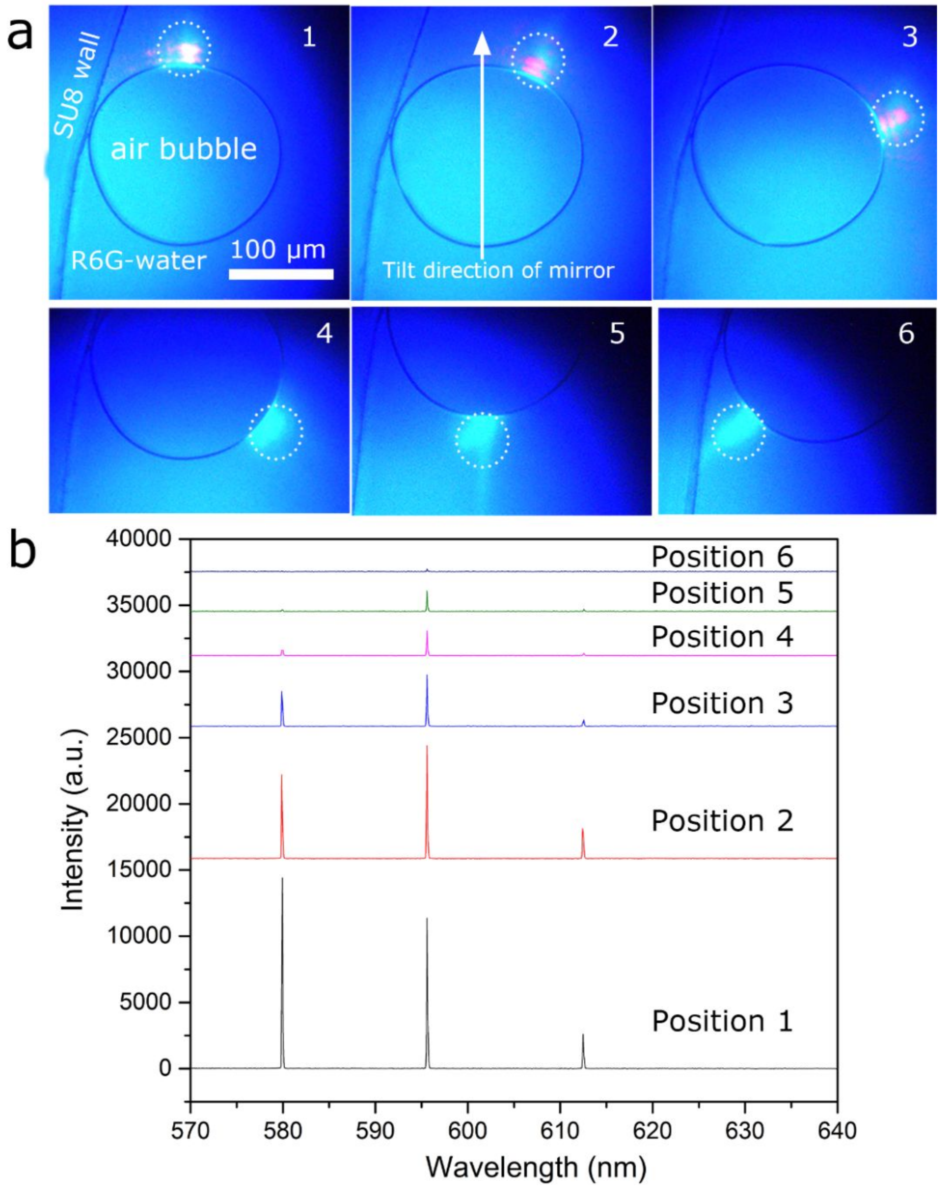

Figure S5. (a) Microscopic images of the TIR-type WFP-DI cavity in Fig. 6a when the pump beam (indicated by the white dotted circle) is moved around the water-air boundary from Position 1 to 6. The pump energy density and the imaging conditions are kept the same. In Position 1-3 (the upper boundary) strong red fringes related to the bouncing ball modes are observed. In contrast, in Position 4-6 (the lower boundary), only very weak lasing emission is observed. Since bouncing ball modes can exist only in the DI Enhanced Region, we can tell that the mirror is tilted approximately along the direction indicated by the white arrow in the second image and the mirror spacing in Position 1-3 is smaller than that in Position 4-6. (b) Corresponding lasing spectra for Position 1-6 in (a) under the same pump energy density (15 μJ/mm^2). Curves are vertically shifted for clarity.

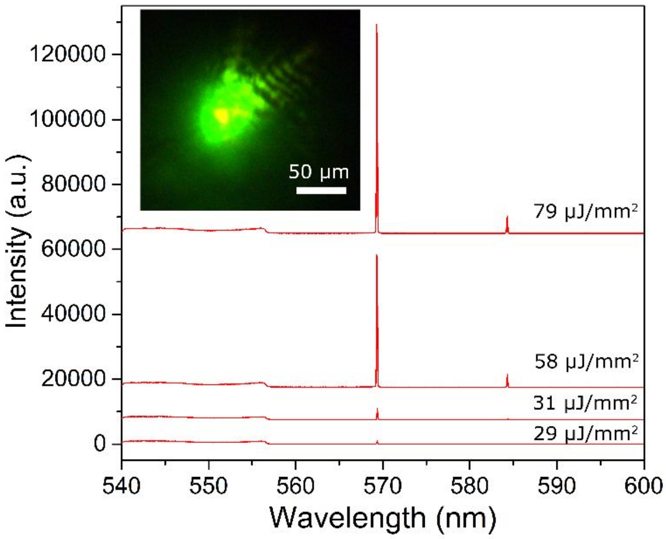

Figure S6. Lasing spectra under different pump energy densities for the WFP cavity without the DI in Fig. 7(c). Curves are vertically shifted for clarity.

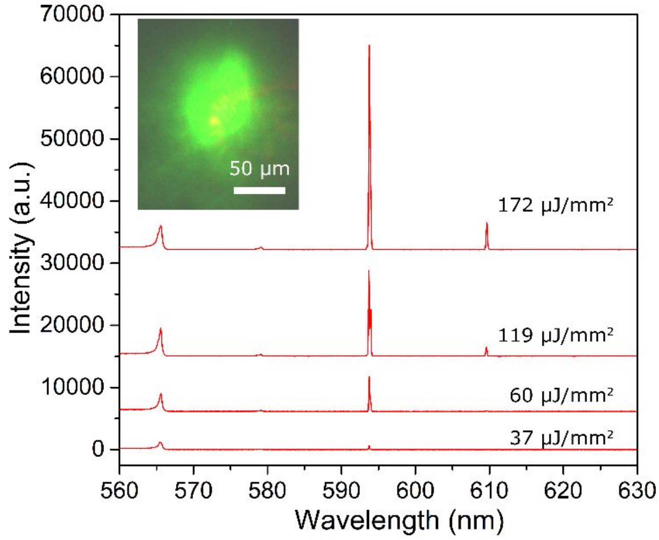

Figure S7. Lasing spectra under different pump energy densities for the WFP cavity without the DI in Fig. 8(c). Curves are vertically shifted for clarity.

Table S1: Parameters used for the calculation of Q-factor from measured lasing threshold I_{th} in Fig. 6e.

Dye concentration N	1 mM (6.02×10^{17} cm^{-3})	
Pump wavelength λ_p (nm)	532	
Absorption cross section at λ_p(cm^2)	3.96×10^{-16}	
Refractive index of the medium n_1	1.33	
Pump pulse width Δt (ns)	5	
Lifetime of R6G (ns)	4.08	
Figure 6e	WFP-DI	WFP
Lasing wavelength λ_L (nm)	595.073	577.102
Absorption cross section at λ_L(cm^2)	1.08×10^{-18}	5.4×10^{-18}
Emission cross section at λ_L(cm^2)	1.07×10^{-16}	1.6×10^{-16}
Mode volume (cm^3)	7×10^{-9}	2.3×10^{-8}
I_{th} ($\mu J/mm^2$)	2	14
Q	2.8×10^4	3.6×10^3

Table S2: Parameters used for the calculation of Q-factor from measured lasing threshold I_{th} in Fig. 7c.

Figure 7c	WFP-DI (Position 1)	WFP-DI (Position 5)	WFP
Lasing wavelength λ_L (nm)	616.401	615.965	569.302
Absorption cross section at λ_L(cm^2)	1.67×10^{-20}	1.67×10^{-20}	9.57×10^{-18}
Emission cross section at λ_L(cm^2)	5.7×10^{-17}	5.7×10^{-17}	1.92×10^{-16}
Mode volume (cm^3)	2.5×10^{-8}	6.3×10^{-8}	2.3×10^{-8}
I_{th} ($\mu J/mm^2$)	1	7	27
Q	9.6×10^4	1.4×10^4	1.9×10^3

Table S3: Parameters used for the calculation of Q-factor from measured lasing threshold I_{th} in Fig. 8c.

Figure 8c	WFP-DI (Position 1)	WFP-DI (Position 2)	WFP
Lasing wavelength λ_L (nm)	606.396	590.058	593.765
Absorption cross section at λ_L(cm^2)	3.57×10^{-19}	1.78×10^{-18}	1.27×10^{-18}
Emission cross section at λ_L(cm^2)	8.17×10^{-17}	1.18×10^{-16}	1.1×10^{-16}
Mode volume (cm^3)	5×10^{-9}	2×10^{-8}	2.3×10^{-8}
I_{th} ($\mu J/mm^2$)	1	14	40
Q	7×10^4	4.8×10^3	3.1×10^3